chinaXiv:201605.01395v1

Structure of *Drosophila* Oskar reveals a novel RNA binding protein

Na Yang[a,b,1,2], Zhenyu Yu[a,1], Menglong Hu[a,1,3], Mingzhu Wang[a], Ruth Lehmann[c,d,2], and Rui-Ming Xu[a,b,2]

[a]National Laboratory of Biomacromolecules, Institute of Biophysics, Chinese Academy of Sciences, Beijing 100101, China; [b]College of Life Sciences, University of Chinese Academy of Sciences, Beijing 100049, China; [c]Howard Hughes Medical Institute, Skirball Institute of Biomolecular Medicine, New York University School of Medicine, New York, NY 10016; and [d]Department of Cell Biology, New York University School of Medicine, New York, NY 10016

Contributed by Ruth Lehmann, August 7, 2015 (sent for review July 16, 2015; reviewed by Anthony P. Mahowald and Dinshaw J. Patel)

Oskar (Osk) protein plays critical roles during *Drosophila* germ cell development, yet its functions in germ-line formation and body patterning remain poorly understood. This situation contrasts sharply with the vast knowledge about the function and mechanism of *osk* mRNA localization. Osk is predicted to have an N-terminal LOTUS domain (Osk-N), which has been suggested to bind RNA, and a C-terminal hydrolase-like domain (Osk-C) of unknown function. Here, we report the crystal structures of Osk-N and Osk-C. Osk-N shows a homodimer of winged-helix–fold modules, but without detectable RNA-binding activity. Osk-C has a lipase-fold structure but lacks critical catalytic residues at the putative active site. Surprisingly, we found that Osk-C binds the 3′UTRs of *osk* and *nanos* mRNA in vitro. Mutational studies identified a region of Osk-C important for mRNA binding. These results suggest possible functions of Osk in the regulation of stability, regulation of translation, and localization of relevant mRNAs through direct interaction with their 3′UTRs, and provide structural insights into a novel protein–RNA interaction motif involving a hydrolase-related domain.

Oskar | structure | RNA-binding | 3′UTR | germ cell

Spatial and temporal control of mRNA localization and translation play critical roles in oocyte development, cell polarity, and neuronal function (1, 2). The assembly of germ plasm in *Drosophila* is illustrative of such strict regulations. During oogenesis, the germ plasm is assembled at the posterior pole of the oocyte. Germ plasm is composed of RNAs and proteins, which are specifically required for the formation of germ cells in the early embryo and specification of germ cell fate (3). Germ plasm is also the source of the Nanos protein gradient required for embryonic polarity. Aberrant mRNA localization and untimely protein synthesis during oogenesis can lead to germ cell formation defects and mis-patterning, causing embryonic lethality and sterility (4).

A critical component of germ plasm is *oskar*. *Oskar* RNA is synthesized during oogenesis in the nurse cells, the sister cells of the oocyte, and transported toward the oocyte's posterior pole by a process involving the exon junction complex, the *oskar* 3′UTR, and microtubule-based movement (5, 6). Oskar protein translation is repressed during transport by the RNA-binding protein Bruno and this repression is released by the binding of activators, such as Orb, once the RNA reaches the posterior pole (7–11). Oskar organizes germ plasm by recruiting other proteins, such as Vasa, Tudor, and Aubergine (12–15). An important function of germ plasm is the localization of 50–200 germ plasm-associated RNAs (16, 17). Among these, *nanos* (*nos*), *germ cell-less* (*gcl*), and *polar granule component* (*pgc*) have important roles in abdominal patterning and germ cell specification, germ cell formation, and germ cell transcriptional repression, respectively (18–22). All these functions fail in the absence of Osk and can be initiated at an ectopic location upon mislocalization of Osk (4, 23).

Germ plasm-associated RNAs are translationally repressed outside of the germ plasm and are translated in the germ plasm or germ cells. Osk has been implicated not only in the localization but also in the translational activation of *nos* mRNA, possibly by releasing the inhibitor Smaug (24). It is not known how Osk disrupts the interaction between Smaug and *nos* 3′UTR and whether Osk is also responsible for translational regulation of other germ plasm-enriched RNAs.

Although the function and the mechanism of *osk* mRNA localization have been studied in great detail, the role of Osk protein in germ-line formation and body patterning remains poorly understood. Translation of *osk* mRNA generates two protein isoforms, a long form and a short Osk protein spanning residues 1–606 and 139–606, respectively. The two isoforms have different localization patterns and the short Osk alone can rescue the defects of *osk* mutants, whereas the long Osk cannot (25). Here we focus our study on the short Osk protein, which is composed of an N-terminal LOTUS/OST-HTH domain (Osk-N) and a C-terminal hydrolase-like domain (Osk-C) (Fig. 1*A*). We have solved the crystal structure of each domain, and our combined structural and biochemical studies offer mechanistic insights into the molecular function of Oskar.

Results

The LOTUS Domain of Osk Is a Winged-Helix–Fold Dimerization Module. An ∼80-residue N-terminal segment of short Osk, termed the LOTUS domain, was predicted to form an RNA-binding domain resembling the structure of a winged-helix DNA-binding domain.

Significance

A profound question in animal biology concerns the origin of germ cells. In the model organism *Drosophila melanogaster*, *oskar* directs the assembly of germ plasm that forms and specifies germ cells, but the precise function of its gene product, the Oskar protein, remains poorly understood. Using X-ray crystallography, we determined the 3D structures of an N-terminal fragment (Osk-N) and a C-terminal domain of Oskar (Osk-C). Surprisingly, we discovered that Osk-C has RNA binding function. It binds the 3′UTR of its own mRNA, as well as that of *nanos*, another gene important for germ-line development. This discovery should direct future mechanistic studies of Oskar for a better understanding of its function in germ cell development.

Author contributions: N.Y., Z.Y., M.H., R.L., and R.-M.X. designed research; N.Y., Z.Y., M.H., and M.W. performed research; N.Y., Z.Y., M.H., M.W., R.L., and R.-M.X. analyzed data; and N.Y., R.L., and R.-M.X. wrote the paper.

Reviewers: A.P.M., The University of Chicago; and D.J.P., Memorial Sloan-Kettering Cancer Center.

The authors declare no conflict of interest.

Freely available online through the PNAS open access option.

Data deposition: Atomic coordinates and diffraction data of the structures have been deposited the Protein Data Bank, www.pdb.org (PDB ID codes 5CD8, 5CD7, and 5CD9 for Osk-N, its L199M mutant, and Osk-C, respectively).

[1]N.Y., Z.Y., and M.H. contributed equally to this work.

[2]To whom correspondence may be addressed. Email: yangna@moon.ibp.ac.cn, Ruth.Lehmann@med.nyu.edu, rmxu@sun5.ibp.ac.cn.

[3]Present address: School of Biomedical Sciences, University of Hong Kong, Hong Kong 999077, China.

This article contains supporting information online at www.pnas.org/lookup/suppl/doi:10.1073/pnas.1515568112/-/DCSupplemental.

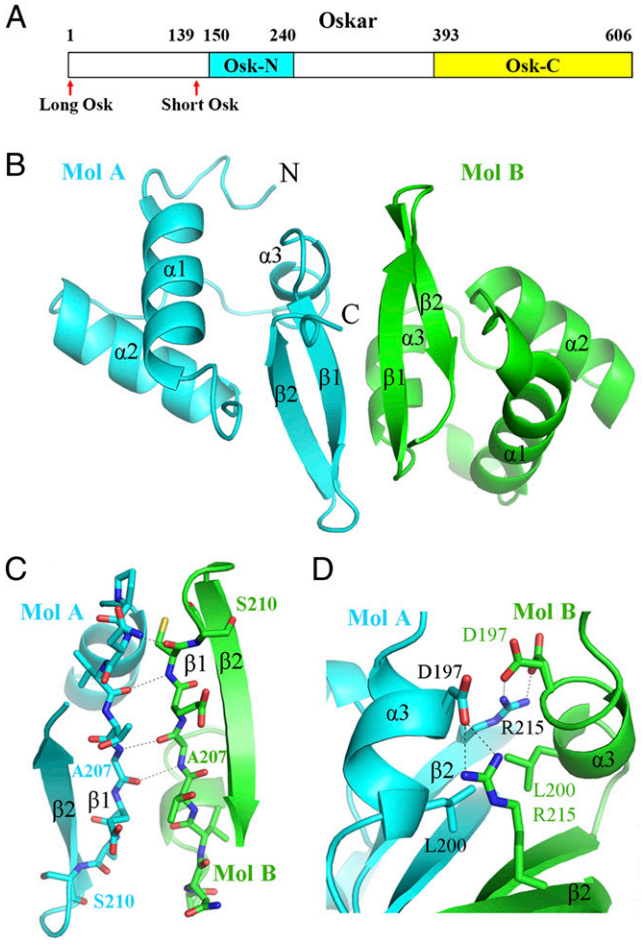

Fig. 1. Structure of Osk-N. (*A*) A schematic drawing of domain organization of Osk. The shaded regions indicate Osk-N (cyan) and Osk-C (yellow). Starting positions of long and short forms of Osk are indicated with red arrows. Residue numbers at domain boundaries are labeled. (*B*) Overall structure of Osk-N homodimer. Two Osk-N molecules, Mol A and Mol B, are shown as a ribbon model colored in cyan and green, respectively. (*C*) Dimerization interactions involving intermolecular hydrogen bonding (dashed lines) between main-chain groups of two β1 stands. β1 stands are shown in a stick model (carbon, cyan and green; nitrogen, blue; oxygen, red; sulfur, yellow). (*D*) Intermolecular interactions between the two α3 helixes. Residues involved in interactions are shown in a stick model.

We crystallized two Osk fragments encompassing the delineated region, one wild-type fragment spanning residues 150–240 and a L199M mutant (animo acids 150–224), which is used for the SeMet-based single wavelength anomalous dispersion (SAD) method of structure determination. The two structures have been determined to 3.0 Å and 2.5 Å, respectively (Table S1). Despite being crystallized in different space groups, there are six protein monomers per asymmetric unit for both the wild-type and the mutant Osk fragments that can be separated into three homodimers with the same protein–protein interaction interface (Fig. S1). Furthermore, the ordered protein regions end within residues 220–223, and there are no significant differences, with an rmsd of 1.5 Å, between the structure models. Thus, the two structures will be collectively referred to as Osk-N henceforth, unless explicitly specified.

The Osk-N monomer adopts a winged-helix–fold, a typical DNA or RNA binding motif, with two antiparallel β-strands (β1 and β2) and three α-helixes (α1–α3) forming the "wing" and "helix," respectively (Fig. 1*B*). Osk-N is predicted to be a RNA-binding motif, termed the LOTUS domain (26, 27). The structure shows that although Osk-N assumes a fold capable of RNA binding, it homodimerizes through the wing and helix α3, masking the potential nucleic acid binding surface (Fig. S2). The dimerization interface buries a total surface area of 881 Å^2, indicating a moderately strong intermolecular interaction. The dimeric interface has an obvious hydrophobic patch involving Leu200 (located on α3) and Ala207 (located on β1) from both monomers. Principal dimerization interactions occur between the two β1-strands through intermolecular hydrogen bonding of main-chain groups (Fig. 1*C*). Ala207 is situated next to the axis of the pseudo twofold symmetry, and they interact with each other through a pair of intermolecular hydrogen bonds between the main-chain carbonyl and amide groups. Ser210 is located in a loop connecting β1 and β2, which appears to be in a location to influence proper positioning of β1. In addition, Arg215 located on β2 interacts with Asp197 located on α3 of the partner monomer (Fig. 1*D*).

To confirm homodimerization of Osk-N in solution, we analyzed the molecular mass of Osk-N (150–224) by multiangle light scattering (MALS). The measured molecular mass of Osk-N (150–224) is 13.2 kDa (Fig. S3*A*), which is ∼54% larger than the calculated molecular weight of 8.55 kDa, suggesting that dimeric and monomeric forms of Osk-N are in equilibrium in solution. To ensure that the dimeric Osk-N results from specific association, we hoped to identify Osk-N mutants that will disrupt the dimerization interaction. Based on the structural information, we designed a S210P mutant of Osk-N, with the expectation that introduction of a proline will alter the main-chain conformation of β1 that leads to the disruption of the dimer. MALS measurements show that S210P has a molecular mass of 8.77 kDa, a value close to the calculated mass of monomeric Osk-N (Fig. S3*A*). This result indicates that the observed Osk-N dimer is a result of specific association of two monomers.

Overall Structure of Osk-C. A 2.1 Å structure of the C-terminal domain of Oskar (Osk-C, amino acids 393–606) was solved, and the structure reveals a globular domain composed of seven α-helices (α1–α7), two β-strands (β1 and β2), and several long loops. β1 is located between α2 and α3, and β2 is inserted between α4 and α5. The two β-strands form a parallel sheet. Three long loops stand out in the structure: they are the N-terminal loop (LN), the one connecting α1 and α2 (L1), and another connecting α6 and α7 (L2) (Fig. 2*A*). These loops are longer than 20 residues and some are embedded with short secondary structural elements. Structural alignment shows that Osk-C has a lipase-like fold, having an rmsd of 2.7 Å when superimposed with a GDSL-like lipase (PDB ID code 3P94). Overall, secondary structural elements (α1–α7 and β1–β2) aligned well between the two structures, but significant differences occur in the loop segments (Fig. 2*B*). The N-terminal ends of Osk-C and the lipase protrude out of the core domain at different directions, and the short turn in the N-terminal loop is replaced by a distorted helix in the lipase structure (Fig. 2*B*). In addition, a pair of short strands—βa preceding α1 and βb between α5 and α6—join β1 and β2 to form an extended β-sheet, and an extra short helix (αa) is found C-terminal to α1 in the lipase structure. Furthermore, the lipase L1 loop and the loop connecting β2 and α5 are longer than the corresponding ones in Osk-C, and these loops take significantly different conformations in the two structures. In contrast, the L2 loop in Osk-C is much longer and extends over a significant portion of the protein surface (Fig. 2*B*).

The catalytic active site of the lipase is located on the loop corresponding to loop L2 in Osk-C. The lipase loop is much shorter, and the catalytic triad residues Ser200, Asp202, and His205 are spatially adjacent. The Osk-C residues corresponding to these positions are Phe571, Leu586, and Phe587 (Fig. 2*B*). Clearly, these hydrocarbon side-chains of the Osk-C residues are incapable to carry out any catalytic activities, as they lack polar functional groups suitable for carrying out nucleophillic attack and electron transfers. Despite the protein-fold similarity, no lipase or similar enzymatic activities are anticipated for Oskar.

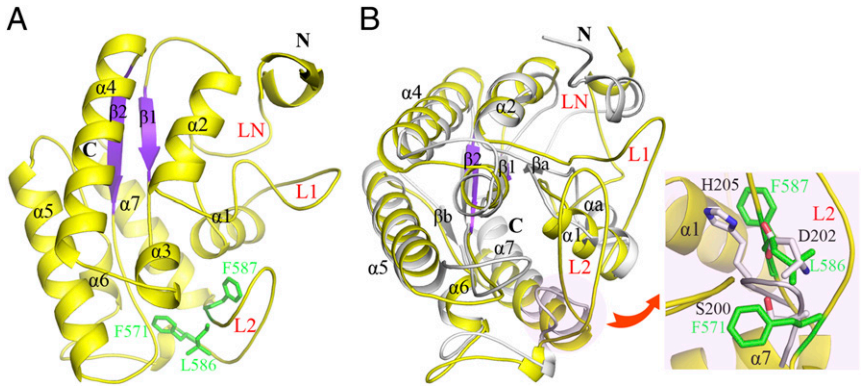

Fig. 2. Structure of Osk-C. (*A*) Overall Structure of Osk-C shown as a ribbon model (α-helixes and loops in yellow and β-sheets in purple). The three long loops are labeled as LN (N-terminal loop), L1 (loop between α1 and α2), and L2 (loop between α6 and α7). (*B*) Structural alignment of Osk-C with a GDSL-like lipase (PDB ID code 3P94). Osk-C is colored the same as in *A* and the lipase is shown in gray. Main differences between the two structures occur in loop regions, notably those of LN, L1, L2, and the one connecting β2 and α5. The area shaded in pink indicates the location of the lipase active site. An enlarged view of the active site is displayed in the pink-shaded inset, in which the catalytic triad of the lipase are highlighted in a stick representation and the corresponding Osk-C residues are shown in green.

RNA Binding Properties of Oskar. Previous studies have shown that the mRNA localization signals of *oskar* and *nanos* are situated in the 3′UTR region of their mRNAs (28, 29). The 3′UTR region often harbors the binding sites of RNA localization and translational control factors. Gene products of *cappuccino*, *orb*, *staufen*, *bruno*, and *oskar* itself, have been implicated as posttranscriptional regulators of *oskar* mRNA (29). For *nanos* mRNA, Smaug and Osk are major regulators for repression and activation of translation (24, 30). However, direct biochemical evidence of Osk as an RNA-binding protein is lacking.

Two incidental observations suggest that Osk-C may be an RNA binding module: (*i*) during protein purification we noticed that Osk-C always associates with nucleic acids; and (*ii*) the protein surface is highly basic, a number of sulfate ions from the crystallization buffer are bound in the structure (Fig. S4). The sulfate ions may mimic the negatively charged phosphate backbone of RNA. Prompted by these observations, we set out to biochemically test the binding of Osk-C and Osk-N fragments to RNA. We first generated the 3′UTR of *osk* mRNA by in vitro transcription, and tested whether Osk-N and Osk-C are able to bind it in an EMSA. The results show that Osk-C binds *osk* 3′UTR avidly, but Osk-N shows no detectable binding under our assay conditions (Fig. 3*A*). Next, we tested whether Osk-C specifically binds RNA or indiscriminately associates with nucleic acids, such as double-stranded DNA (dsDNA), using a competition assay. We generated a fluorescein-labeled *osk* 3′UTR by incorporation of fluorescein-12 dUTP into the probe during in vitro transcription (Fig. 3*B*). Addition of fourfold excess of unlabeled *osk* 3′UTR completely abolished the binding of labeled RNA, whereas dsDNA could not compete for binding even at eightfold excess. Therefore, we conclude that Osk-C is an RNA binding domain that can interact with its own 3′UTR. We further tested the binding of Osk-C to the 3′UTRs of *nos* and *pgc* (Fig. 3*C*). Osk-C bound to the translational control element (TCE) of *nos* 3′UTR, but not to the 3′UTR of *pgc* under the same assay condition and a protein:RNA molar ratio up to 30:1. Osk-C appeared to bind to the 3′UTR of *nos* stronger than to that of *oskar* (Fig. 3*C*). By increasing the protein to RNA ratio we could detect a shift of the 3′UTR of *pgc*, but the implication is unclear. It should be emphasized that our observation does not exclude the possibility that Osk-C may bind full-length *pgc* vigorously.

RNA Binding Surface of Osk-C. The structure of Osk-C reveals several positively charged patches on the surface that may be RNA binding sites (Fig. 4*A*). We chose the residues forming positively charged patches and involved in binding sulfate ions for mutational studies. Eleven single or combinational substitution mutants—R448E, R470E, R490E, R567E, R576E, R593E, R593A, R595E, R436E/R442E, R445E/H446D, and R538E/K541E/R544E—were generated. We were able to express and purify all but the R593E mutant, and they were subjected to EMSA analysis using *oskar* and *nanos* 3′UTRs as probes (Fig. 4*B* and Fig. S5). Compared with wild-type Osk-C, two mutants, R436E/R442E and R576E, showed reduced affinities toward *oskar* 3′UTR. R436E/R442E almost completely lost the ability to bind *oskar* 3′UTR. Similar levels of reduction of binding abilities of these two mutants toward *nos* 3′UTR were observed (Fig. 4*C*). This analysis identifies the regions occupied by the three residues, Arg436, Arg442, and Arg576 as part of the RNA binding surface. Arg436 is located on α1, and Arg442 and Arg576 are situated in the long loops between α1 and α2 and α5 and α6, respectively. These three residues lie on the same side of the Osk-C surface on a positively charged narrow ridge, which appears adequate for accommodating RNA (Fig. 4*D*).

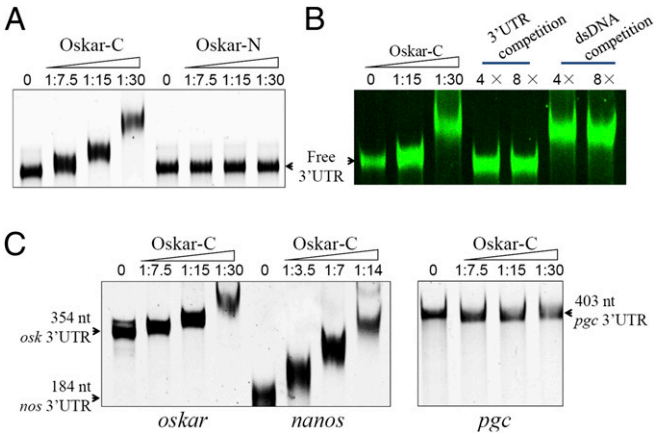

Fig. 3. EMSA analysis of Osk-RNA interaction. (*A*) EMSA results show that Osk-C binds *osk* 3′UTR but Osk-N shows no detectable binding. (*B*) Fluorescein-labeled *osk* 3′UTR, shows as green bands, shifted by increasing concentration of Osk-C and the binding is competed by fourfold-excess of unlabeled *osk* 3′UTR but not dsDNA, even at eightfold excess. (*C*) Binding of Osk-C to the 3′UTRs of *osk,* TCE of *nanos*, and *pgc*.

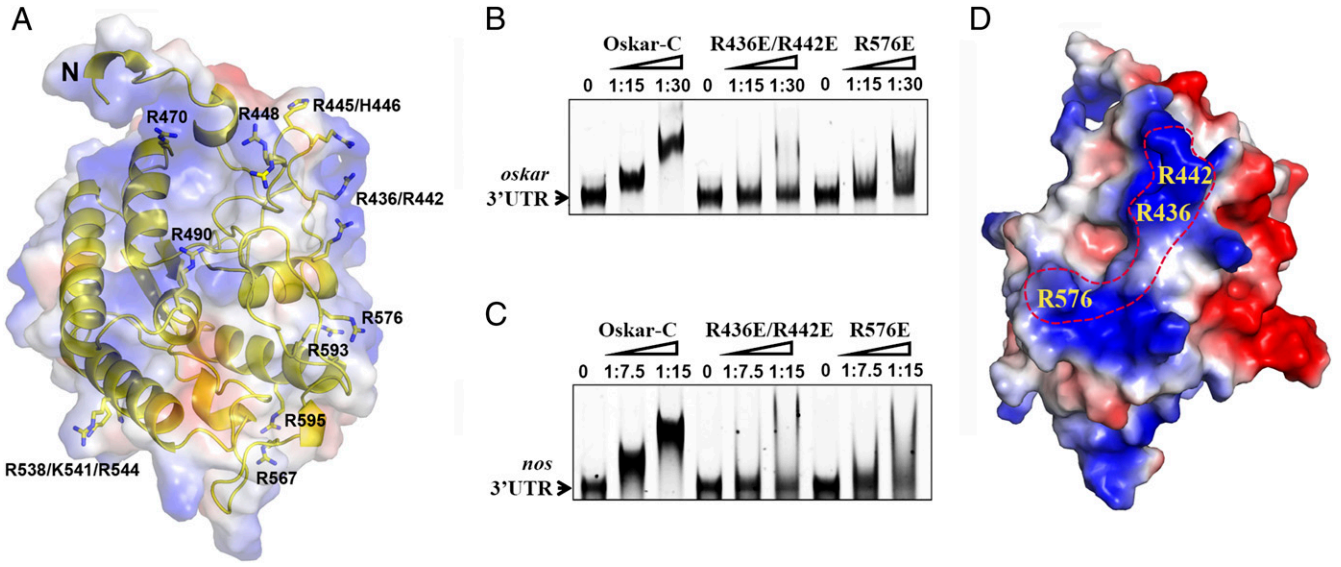

Fig. 4. RNA binding surface of Osk-C. (*A*) Positively charged residues on Osk-C surface selected for mutational analyses are shown in a stick model superimposed with the surface representation of Osk-C colored according to electrostatic potential distribution. (*B* and *C*) Two Osk-C mutants, R436E/R442E and R576E, displayed reduced binding affinity toward the 3′UTRs of *osk* (*B*) and *nanos* (*C*), compared with that of wild-type Osk-C. (*D*) Arg436, Arg442, and Arg576 form a narrow positively charged ridge, which may be involved in RNA binding.

Discussion

Osk is critically important for germ cell development in *Drosophila*. Most studies to date have focused on the function and regulation of *osk* mRNA, and little is known about the biochemical function of Osk protein. It has been reported that Osk interacts with Vasa, Staufen, and Tudor proteins (12), but we were not able to detect robust interactions between Osk and these proteins in our hands by coelution in a gel-filtration column using purified proteins (Fig. S6). Speculations regarding the biochemical properties of Osk from bioinformatic analyses predicted Osk-C to have a hydrolase-like fold and Osk-N to form a LOTUS winged-helix domain with RNA binding properties. Our structural analysis largely confirms the protein-fold predictions, and offers additional and novel insights into the structure and function of Osk. First, the winged-helix LOTUS domain forms a dimer and displays no detectable RNA binding activity. We also do not detect RNA binding activity of monomeric Osk-N using the S210P mutant (Fig. S3*B*). However, it should be cautioned that we could not absolutely rule out possible RNA binding activities of Osk-N because we only tested a specific set of RNAs. The role of the LOTUS domain and the function of the predicted Oskar protein dimer need yet to be determined in vivo. Besides stop codon mutations that lead to protein truncations, specific point mutations mapping to this region and affecting Oskar's posterior patterning function have not been identified.

It comes as a surprise that Osk-C binds RNA. To our knowledge, this is the first time that a lipase-like domain has been reported to be a nucleic acid binding domain. Interestingly, a number of metabolic enzymes have recently been shown to "moonlight" as RNA binding proteins (31). We further find that the 3′UTRs of *osk* and *nanos* are potential binding partners of Osk-C. This discovery provides new insights into the biochemical functions of Oskar in embryonic patterning and germ cell development. Mutational studies also identified surface regions of Osk-C that are important for RNA binding. Interestingly, the biochemically identified residues that are key for RNA binding are in proximity to several genetically identified *osk* alleles defective in posterior pattering (Fig. S7 and Table S2) (32–35). This correlation provides a possible link between the biochemical and developmental functions of Oskar. To gain further insights into the RNA binding property of Osk, we attempted to determine the RNA sequence specificity for Osk-C binding. However, we were unable to discern a pattern by simple deletion analysis. It is possible that there may not be strict RNA sequence specificity for Osk binding, as other factors, such as RNA secondary structures, may regulate RNA binding. Nevertheless, a clearer picture of RNA binding, including a structure of Osk in complex with RNA, should greatly benefit mechanistic understandings of the biological functions of Osk.

Experimental Procedures

Protein Expression and Purification. The short isoform of Oskar, generated from translation initiated from an internal start codon, spans residues 139–606. cDNA fragments encoding Osk-N (residues 150–240) and a L199M mutant (residues 150–224) were cloned into a pET28a-SUMO vector between the BamHI and SalI sites and expressed in the BL21-Codon Plus (DE3)-RIL strain of *Escherichia coli*. Once the cell density reached OD_{600} ∼0.8, protein expression was induced with 0.3 mM isfopropyl-β-D-thiogalactopyranoside (IPTG) at 16 °C for 18 h. Cells were harvested by centrifugation at 4,670 × *g* and lysed by passing through an Emulsiflex C3 cell disruptor in the lysis buffer (20 mM Tris·HCl pH 8.0, 500 mM NaCl, 10 mM imidazole). The homogenate was centrifuged at 26,400 × *g* and supernatant was loaded onto a Ni-NTA (Novagen) column pre-equilibrated with the lysis Buffer. After extensive washing with the washing buffer (20 mM Tris·HCl pH 8.0, 500 mM NaCl, 20 mM imidazole), the his-SUMO tagged protein was eluted with the elution buffer (20 mM Tris·HCl pH 8.0, 500 mM NaCl, 500 mM imidazole). The his-SUMO tag was cleaved with SUMO protease during dialysis against buffer A (20 mM MES pH 6.0, 100 mM NaCl, 0.1% β-ME). The tag-free protein was loaded onto a heparin column pre-equilibrated with buffer A and eluted with a 100–1,000 mM NaCl gradient. The desired fractions were pooled, concentrated and further purified on a Superdex 75 10/60 XK column (GE Healthcare) in a buffer containing 20 mM Tris·HCl pH 8.0, 500 mM NaCl, and 0.1% β-ME.

Osk-C and its mutants were expressed using a modified pET28a-SUMO vector with the coding sequences inserted between the BamHI and SalI sites. Protein expression and purification follow the same procedures as that for Osk-N, except that buffer A used in the Heparin column contains 20 mM Tris·HCl pH 8.0, 150 mM NaCl, 0.1% β-ME, 0.5 mM EDTA, and the final step of size-exclusion column chromatography was carried out using a Superdex 75 10/300 GL column (GE Healthcare) in a buffer containing 20 mM Tris·HCl pH 8.0, 300 mM NaCl, 0.1% β-ME, and 0.5 mM EDTA.

Crystallization and Structure Determination. Osk-N concentrated to ∼5 mg/mL was crystallized using a reservoir buffer containing 100 mM sodium acetate

pH 5.6, 20% (vol/vol) PEG 400 and 200 mM magnesium acetate by hanging-drop vapor diffusion at 16 °C. The L199M mutant was concentrated to 6.5 mg/mL and the crystallization buffer contains 100 mM sodium acetate pH 5.6, 17–22% (vol/vol) PEG 3350 and 150 mM NaCl. Osk-C was concentrated to ~15 mg/mL and crystals for X-ray diffraction were obtained from a condition containing 100 mM sodium acetate pH 4.6, 800 mM ammonium sulfate and 200 mM lithium sulfate, also by hanging-drop vapor diffusion at 16 °C.

X-ray diffraction data were collected at Beamline BL17U of Shanghai Synchrotron Radiation Facility using an ADSC Q315r detector. All diffraction data were processed using HKL2000 (36). The 2.5 Å SAD data for the SeMet L199M mutant were collected at wavelength 0.9790 Å. The crystal belongs to the P21 space group and there are six molecules in one asymmetric unit. The 2.1 Å SAD data of SeMet Osk-C were collected at wavelength 0.9788 Å. The crystal belongs to the P3121 space group and there is one molecule per asymmetry unit. In both cases, six Se sites were found using SHELXD (37) and phasing was carried out with PHENIX (38). A 3.0 Å dataset of SeMet wild-type Osk-N (150–240) was collected at wavelength 0.9641 Å. The crystal belongs to the P32 space group and there are six molecules in one asymmetric unit. The structure was solved by molecular replacement with PHASER (39) using the L199M structure as the search model. Initial model building, model fitting, and refinement of all of the three structures were done with PHENIX and COOT (40). Detailed statistics for data collection and refinement are shown in Table S1.

MALS. Osk-N was diluted to 2 mg/mL in a buffer containing 20 mM Tris·HCl pH 8.0 and 150 mM NaCl. After being centrifuged at 15,871 × *g* for 15 min, a 50-μL sample was loaded onto a WTC-030S5 size-exclusion column (Wyatt Technologies) connected to a MALS instrument (DAWN HELEOS II; Wyatt Technologies). Molecular mass of particles in a single elution peak was calculated based on light scattering data using the ASTRA software package.

In Vitro Transcription of RNA. cDNAs encoding *osk* 3′UTR, *nanos* 3′UTR, and *pgc* 3′UTR were cloned into a pBluescript II SK(+) vector between KpnI and HindIII sites for in vitro transcription. The recombinant plasmid DNAs were linearized with HindIII downstream of the insert to be transcribed as the template. The RNAs were transcribed with T7 polymerase by MEGAscript Kit (AM1334, Ambion) following the procedures recommended by the manufacturer. For in vitro transcription of fluorescein-labeled *osk* 3′UTR, fluorescein-12-UTP (Roche) was added in the reaction together with the unlabeled one. The transcribed RNAs were purified with MEGAclear Purification Kit (Ambion). Quality and quantity of RNAs were examined both by UV spectroscopy and 5% denaturing polyacrylamide gel.

EMSA. In each EMSA reaction (total volume, 20 μL), an 80 ng heat-denatured RNA probe of *osk* 3′UTR, *nanos* 3′UTR, or *pgc* 3′UTR was incubated individually with various quantities of Osk or Osk mutants in a binding buffer containing 20 mM Tris·HCl, pH 7.9, 1 mM DTT, 10 mM KCl, 15 mM NaCl, 40 μg/mL calf BSA, and 5% glycerol for 30 min on ice. After incubation, protein-bound and free RNAs were separated by electrophoresis on nondenaturing 6% polyacrylamide gels (80:1) running in a 0.5×TBE buffer at 10 V/cm^{-1} at 4 °C. For unlabeled RNA probes, gels were stained by SYBR Gold (Life Technologies) and scanned by FluorChem M System (ProteinSimple). For fluorescein-labeled RNAs, gels were directly scanned at 607 nm by FluorChem M System (ProteinSimple). The RNA probes were quantified by UV spectrophotometer Nanodrop 2000 (Thermo Scientific) at wavelength 260 nm.

Accession Numbers. Atomic coordinates and diffraction data of the structures have been deposited with PDB under accession codes 5CD8, 5CD7 and 5CD9 for Osk-N, its L199M mutant, and Osk-C, respectively. Structural figures were prepared using Pymol (www.pymol.org).

Note Added in Proof. While this manuscript was being reviewed, a report by Jeske et al. describing similar studies of Osk was published online (41). Crystal structures of Osk fragments equivalent to Osk-N and Osk-C denoted in our work were reported, and the structures are nearly identical (rmsd 0.34 Å and 0.69 Å for Osk-C and Osk-N, respectively), supporting the dimeric form of Osk-N from both of our studies. Using UV cross-linking and immunoprecipitation, Jeske et al. (41) showed that full-length short Oskar binds to *nos*, *pgc*, and *gcl* mRNAs in vivo, and the RNA binding activity was attributed to Osk-C based on in vitro pulldown results. In our work, we showed that purified Osk-C directly binds the 3′UTR regions of *osk* and *nos* in vitro. We detected no meaningful binding of Osk-C to the 3′UTR of *pgc* in our assay, but we cannot rule out that Osk-C may bind full-length *pgc* mRNA. Another difference between the two studies is that Osk-N was shown to interact with Vasa by Jeske et al. using GST-pulldown, isothermal titration calorimetry, and yeast two-hybrid assays. We were not able to detect such interaction by gel-filtration column chromatography using purified proteins.

ACKNOWLEDGMENTS. We thank the beamline scientists at Shanghai Synchrotron Radiation Facility for technical support during data collection; Xiaoxia Yu for assistance with mulitangle light-scattering experiments; and Dr. Thomas Hurd for critically reading the manuscript. This work was supported by the Natural Science Foundation of China (Grants 31370734, 31430018, and 31400670); the Ministry of Science and Technology of China (Grant 2015CB856202); the National Key New Drug Creation and Manufacturing Program of China (Grant 2014ZX09507002); the Strategic Priority Research Program (Grant XDB08010100); and the Key Research Program (Grant KJZDEW-L05) of the Chinese Academy of Sciences. N.Y. is also supported by the Youth Innovation Promotion Association of the Chinese Academy of Sciences. R.L. is a Howard Hughes Medical Institute investigator.

1. Besse F, Ephrussi A (2008) Translational control of localized mRNAs: Restricting protein synthesis in space and time. *Nat Rev Mol Cell Biol* 9(12):971–980.
2. Kugler JM, Lasko P (2009) Localization, anchoring and translational control of oskar, gurken, bicoid and nanos mRNA during *Drosophila* oogenesis. *Fly (Austin)* 3(1):15–28.
3. Mahowald AP (2001) Assembly of the *Drosophila* germ plasm. *Int Rev Cytol* 203: 187–213.
4. Ephrussi A, Lehmann R (1992) Induction of germ cell formation by oskar. *Nature* 358(6385):387–392.
5. Ghosh S, Marchand V, Gáspár I, Ephrussi A (2012) Control of RNP motility and localization by a splicing-dependent structure in oskar mRNA. *Nat Struct Mol Biol* 19(4): 441–449.
6. Zimyanin VL, et al. (2008) In vivo imaging of oskar mRNA transport reveals the mechanism of posterior localization. *Cell* 134(5):843–853.
7. Kim-Ha J, Kerr K, Macdonald PM (1995) Translational regulation of oskar mRNA by bruno, an ovarian RNA-binding protein, is essential. *Cell* 81(3):403–412.
8. Chekulaeva M, Hentze MW, Ephrussi A (2006) Bruno acts as a dual repressor of oskar translation, promoting mRNA oligomerization and formation of silencing particles. *Cell* 124(3):521–533.
9. Chang JS, Tan L, Schedl P (1999) The *Drosophila* CPEB homolog, orb, is required for oskar protein expression in oocytes. *Dev Biol* 215(1):91–106.
10. Kim G, et al. (2015) Region-specific activation of oskar mRNA translation by inhibition of Bruno-mediated repression. *PLoS Genet* 11(2):e1004992.
11. Nakamura A, Sato K, Hanyu-Nakamura K (2004) *Drosophila* cup is an eIF4E binding protein that associates with Bruno and regulates oskar mRNA translation in oogenesis. *Dev Cell* 6(1):69–78.
12. Breitwieser W, Markussen FH, Horstmann H, Ephrussi A (1996) Oskar protein interaction with Vasa represents an essential step in polar granule assembly. *Genes Dev* 10(17):2179–2188.
13. Lasko P (2011) Posttranscriptional regulation in *Drosophila* oocytes and early embryos. *Wiley Interdiscip Rev RNA* 2(3):408–416.
14. Anne J (2010) Targeting and anchoring Tudor in the pole plasm of the *Drosophila* oocyte. *PLoS One* 5(12):e14362.
15. Thomson T, Liu N, Arkov A, Lehmann R, Lasko P (2008) Isolation of new polar granule components in *Drosophila* reveals P body and ER associated proteins. *Mech Dev* 125(9-10):865–873.
16. Jambor H, et al. (2015) Systematic imaging reveals features and changing localization of mRNAs in *Drosophila* development. *eLife* 4:e05003.
17. Lécuyer E, et al. (2007) Global analysis of mRNA localization reveals a prominent role in organizing cellular architecture and function. *Cell* 131(1):174–187.
18. Wang C, Lehmann R (1991) Nanos is the localized posterior determinant in *Drosophila*. *Cell* 66(4):637–647.
19. Cinalli RM, Lehmann R (2013) A spindle-independent cleavage pathway controls germ cell formation in *Drosophila*. *Nat Cell Biol* 15(7):839–845.
20. Jongens TA, Hay B, Jan LY, Jan YN (1992) The germ cell-less gene product: A posteriorly localized component necessary for germ cell development in Drosophila. *Cell* 70(4):569–584.
21. Hanyu-Nakamura K, Sonobe-Nojima H, Tanigawa A, Lasko P, Nakamura A (2008) *Drosophila* Pgc protein inhibits P-TEFb recruitment to chromatin in primordial germ cells. *Nature* 451(7179):730–733.
22. Martinho RG, Kunwar PS, Casanova J, Lehmann R (2004) A noncoding RNA is required for the repression of RNApolII-dependent transcription in primordial germ cells. *Curr Biol* 14(2):159–165.
23. Smith JL, Wilson JE, Macdonald PM (1992) Overexpression of oskar directs ectopic activation of nanos and presumptive pole cell formation in *Drosophila* embryos. *Cell* 70(5):849–859.
24. Dahanukar A, Walker JA, Wharton RP (1999) Smaug, a novel RNA-binding protein that operates a translational switch in *Drosophila*. *Mol Cell* 4(2):209–218.
25. Markussen FH, Michon AM, Breitwieser W, Ephrussi A (1995) Translational control of oskar generates short OSK, the isoform that induces pole plasma assembly. *Development* 121(11):3723–3732.
26. Callebaut I, Mornon JP (2010) LOTUS, a new domain associated with small RNA pathways in the germline. *Bioinformatics* 26(9):1140–1144.
27. Anantharaman V, Zhang D, Aravind L (2010) OST-HTH: A novel predicted RNA-binding domain. *Biol Direct* 5:13.

28. Gavis ER, Lehmann R (1994) Translational regulation of nanos by RNA localization. *Nature* 369(6478):315–318.
29. Rongo C, Lehmann R (1996) Regulated synthesis, transport and assembly of the *Drosophila* germ plasm. *Trends Genet* 12(3):102–109.
30. Dahanukar A, Wharton RP (1996) The Nanos gradient in *Drosophila* embryos is generated by translational regulation. *Genes Dev* 10(20):2610–2620.
31. Castello A, et al. (2012) Insights into RNA biology from an atlas of mammalian mRNA-binding proteins. *Cell* 149(6):1393–1406.
32. Lehmann R, Nüsslein-Volhard C (1986) Abdominal segmentation, pole cell formation, and embryonic polarity require the localized activity of *oskar*, a maternal gene in *Drosophila*. *Cell* 47(1):141–152.
33. Ephrussi A, Dickinson LK, Lehmann R (1991) Oskar organizes the germ plasm and directs localization of the posterior determinant nanos. *Cell* 66(1):37–50.
34. Kim-Ha J, Smith JL, Macdonald PM (1991) oskar mRNA is localized to the posterior pole of the *Drosophila* oocyte. *Cell* 66(1):23–35.
35. Rongo C (1996) The role of RNA localization and translational regulation in *Drosophila* germ cell determination. PhD thesis (Massachusetts Institute of Technology, Cambridge, MA).
36. Otwinowski Z, Minor W (1997) Processing of X-ray diffraction data collected in oscillation mode. *Methods Enzymol* 276:307–326.
37. Sheldrick GM (2008) A short history of SHELX. *Acta Crystallogr A* 64(Pt 1):112–122.
38. Adams PD, et al. (2010) PHENIX: A comprehensive Python-based system for macromolecular structure solution. *Acta Crystallogr D Biol Crystallogr* 66(Pt 2):213–221.
39. Collaborative Computational Project, Number 4 (1994) The CCP4 suite: Programs for protein crystallography. *Acta Crystallogr D Biol Crystallogr* 50(Pt 5):760–763.
40. Emsley P, Cowtan K (2004) Coot: Model-building tools for molecular graphics. *Acta Crystallogr D Biol Crystallogr* 60(Pt 12 Pt 1):2126–2132.
41. Jeske M, et al. (2015) The crystal structure of the *Drosophila* germline inducer Oskar identifies two domains with distinct Vasa helicase- and RNA-binding activities. *Cell Reports* 12(4):587–598.